INL/JOU-24-81195-Revision-0

Transmission Electron Microscopy Characterization of Fuel-Cladding Chemical Interaction between U-Pu-Zr fuel with Added Minor Actinides and AIM1 Cladding

Di Chen, Jatuporn Burns, Karen E Wright, Tiankai Yao, Luca Capriotti

Changing the World's Energy Future

Idaho National Laboratory

INL is a U.S. Department of Energy National Laboratory operated by Battelle Energy Alliance, LLC

INL/JOU-24-81195-Revision-0

Transmission Electron Microscopy Characterization of Fuel-Cladding Chemical Interaction between U-Pu-Zr fuel with Added Minor Actinides and AIM1 Cladding

Di Chen, Jatuporn Burns, Karen E Wright, Tiankai Yao, Luca Capriotti

March 2025

Idaho National Laboratory
Idaho Falls, Idaho 83415

http://www.inl.gov

Prepared for the
U.S. Department of Energy
Under DOE Idaho Operations Office
Contract DE-AC07-05ID14517

Transmission Electron Microscopy Characterization of Fuel Cladding Chemical Interaction between Minor Actinides bearing U-Pu-Zr Fuel and AIM1 Cladding

Di Chen, Jatuporn Burns, Karen E. Wright, Daniele Salvato,

Tiankai Yao*, and Luca Capriotti*

Idaho National Laboratory, Idaho Falls, ID, 83415, US

*Corresponding authors.

Abstract

Minor actinides (MA) significantly contribute to the long-term radiotoxicity of spent nuclear fuel (SNF). Separating MA from SNF and incorporating it into metallic fuels for fast reactor transmutation is a potential method to reduce this radiotoxicity. This study focuses on transmission electron microscopy characterization of two samples from the fuel cladding chemical interaction (FCCI) region of an americium (Am) and neptunium (Np)-bearing (MA-bearing) uranium-plutonium-zirconium (U-Pu-Zr) fuel irradiated in the Phenix fast reactor to 9.5 % FIMA burnup at approximately 550 ˚C cladding temperature. The results show that despite the complex chemical interactions between MA and AIM1 cladding elements, excessive FCCI was not induced, and Am penetration depth in the cladding limited to less than 4 μm. Np remained mostly inside fuel. The Zr-rich compounds layer effectively limited the accumulation of lanthanide on the inner cladding surface. Overall, the FCCI behavior between investigated MA-bearing U-Pu-Zr fuel and AIM1 cladding is benign.

1. Introduction

Managing high-level radioactive nuclear waste from irradiated oxide fuel in light water reactors is challenging due to the presence of long- lived minor actinides (MA). These MA increase radiotoxicity and heat load of the nuclear waste, complicating its disposal. One promising solution is separating MA, such as neptunium-237, americium-241, and curium-244, from spent nuclear fuel (SNF) and reprocessing them into fuel forms for fast reactors so that they can be transmuted to other nuclides with lower radiotoxicity [1–3].

U-xPu-10Zr metallic fuel has high uranium density with potential to be recycled using pyro processing [4].

The Fuel for Transmutation of transuranium elements in phenIX- Fortes Teneurs en Actinides (FUTURIX-FTA) is an international research project focused on studying the transmutation of MA through irradiation. The FUTURIX-FTA experiment is a collaborative effort involving the U.S. DOE and the French Commissariat a l` ·Energie ´ Atomique et aux Energies Alternatives

(CEA). Through this collaboration, the project aims to enhance the understanding of MA transmutation processes in metallic fuel. As part of the project, this experiment aimed to investigate the behavior of U-Pu-Zr fuels bearing MA under fast reactor operating conditions. The subsequent post- irradiation examinations (PIE) of these experiments will provide a better understanding of fuel performance, serving as the scientific basis for designing transmutation fuels [5–7].

Fuel cladding chemical interaction (FCCI) is a potential life limiting factor for metallic fuels in fast reactors, as it significantly affects fuel performance and longevity [8]. FCCI involves chemical reactions at the interface between the fuel and cladding, leading to cladding wastage, which can compromise the cladding's structural integrity [9].

Studies of the U-Pu-Zr subassembly X447 provide crucial insights into the mechanisms driving FCCI, particularly through the development of the three-zone model of constituent redistribution [10–13]. Additionally, research conducted under the METAPHIX project further highlights the redistribution of MA and the formation of secondary phases within the fuel [14–15], emphasizing the impact of MA on FCCI.

A previous EPMA study [16] demonstrated both significant MA redistribution in U-Pu-Zr fuel and notable FCCI phenomena. While the center of the fuel remained mostly a single phase, the periphery split into a (U, Np, Pu)Zr_2-like phase and a high-U, low-Zr phase. Am, lanthanides, and actinides precipitated in a $Nd_7(Pd, Rh)_3$-like phase near the outer fuel radius, with Am also dissolving into major fuel phases. In the most severe case, Sm and Am penetrated up to 15 µm into the AIM1 cladding, while Fe, Ni, and Cr from the cladding penetrated up to 30 µm into the fuel.

This study, through comprehensive scanning electron microscopy (SEM), transmission electron microscopy (TEM), and energy-dispersive x-ray spectroscopy (EDS) mapping analyses, aims at elucidating the microstructural and elemental interactions at two selected fuel-cladding interface sites with following research focuses:

- Microstructure and phase characterization at micro- and nanoscale (SEM and TEM).
- Elemental distribution of key elements particularly Am and Sm within the FCCI and adjacent regions.
- Phase identification by indexing the collected selected area electron diffraction patterns.
- Diffusion mechanisms of MA and other elements into the cladding and their impact on FCCI. This includes studying the penetration depth and clustering behavior of MA and lanthanide fission products and their interactions with cladding elements such as Fe, Ni, and Cr.
- The implications of results on FCCI and MA-bearing metal fuel performance in fast reactors.

2. Experiments

2.1.Fuel fabrication

The fuel fabrication process, as detailed by Ref. [17], was used to create 4.9 mm diameter cylindrical fuel slugs. This process began by melting metallic feedstocks to form a homogenized button. The button underwent at least three cycles of melting and solidifying to ensure homogeneity. After homogenization, the charge was remelted and drawn up via suction

into quartz mold. The resulting slugs varied in length, with an average length of approximately 100.0 ± 1.0 mm. Using a combination of inductively-coupled plasma - mass spectrometry (ICP-MS) and ICP - atomic emission spectrometry (ICP-AES) [16], the composition of the as-fabricated fuel slugs was determined to be 34.1U-28.3Pu-3.8Am-2.1Np-31.7Zr by weight percent, which corresponds to approximately 22.6U-18.6Pu-1.42Np-2.52Am-54.9Zr in atomic percent.

The fuel slugs were encased in AIM1 cladding, a 316 stainless steel with a estimated composition in weight % of 14–16Cr, 14–16Ni, 1–2Mn,1.3–1.7Mo, 0.7–0.9Si, 0.3–0.5Ti 0.08–0.1C and Fe Matrix [18, 19].

2.2. Irradiation

The encased fuel slugs were irradiated in the Phenix sodium fast ′ reactor, operating at an average linear heat generation rate of 318 W/ cm. The temperature of the cladding reached 550 °C, and the DOE1 fuel achieved a fission density of 2.08×10^{21} f/cm³, equivalent to 9.5 at % FIMA [16].

2.3. Post irradiation examination

2.3.1. Rodlet sectioning and polishing

The irradiated fuel slugs were sectioned in Hot Fuel Examination Facility (HFEF) at INL. The transverse cross-sectional sample was cut at height of x/L = 0.5 using low-speed diamond saw. The sample was mounted in epoxy and polished for metallographic examination.

2.3.2. Site-specific TEM sample preparation

A focused ion beam (FIB) scanning electron microscopy (SEM) at the Irradiated Materials Characterization Laboratory (IMCL) in INL was used to extract two lamellae at two FCCI sites. The lamellae were thinned to electron transparency for TEM characterization.

2.3.3. TEM characterization

Titan Themis TEM at INL's IMCL [20] was used to study the microstructural and phase characteristics of the FCCI region. The TEM analysis included bright-field TEM (BF-TEM) imaging of grain boundaries, phase precipitates, and voids. STEM-EDS analysis involved scanning TEM (STEM) coupled with EDS providing high-resolution elemental maps and line scans for chemical elements at the nanoscale.

3. Results

Fig. 1 shows an area of interest for FCCI research (1a), the position identified for a FIB lamella lift-out (1b), the pre-thinned lamella (1c), and the thinned lamella (1d). Fig. 1c provides an overview of the extracted lamella sample, including both the fuel and cladding sections.

Fig. 2 provides an in-depth TEM chemical analysis of the entire sample prepared inside the FCCI region, using the Velox software for analysis. Fig. 2a shows different microstructure features between fuel and cladding.

Fig. 2b presents the corresponding STEM-EDS mapping, illustrating the distributions of key elements (Si, Ti, Cr, Fe, Ni, Zr, Ce, Sm, U, Pu, and Am) across the FCCI region. The map uses different colors to represent areas where specific elements were concentrated. This color-coded mapping provides a clear visualization of the spatial distribution and relative concentration of each element within the FCCI region. The arrow with the white box indicates the specific area analyzed for one- dimensional element distribution, as will be shown in Fig. 3. The cladding region, highlighted by the green box in Fig. 2a, is shown in detail in Fig. 2c. This zoomed-in view shows the distribution of all key elements, both overlaid and as single elements, within the cladding. All elements, except Ti, formed clusters near the interface within the FCCI region. Ti, on the other hand, formed small clusters in the cladding away from the FCCI region. In Fig. 2c, the STEM-EDS mapping revealed a very small amount of diffusion of U and Pu into the cladding. However, Am and Sm, confirmed by integrated STEM-EDS spectrum in Fig. 2d, penetrated the cladding to a depth of 2–3 μm and formed submicron sized clusters. Lanthanide fission products other than Sm, represented by Ce, remained inside the Zr-rich compounds layer at the fuel side.

Fig. 3a illustrates the one-dimensional distribution of elements from the fuel to the cladding, as indicated by the arrow in Fig. 2b, along with a quantitative analysis.

The black box in Fig. 3a highlights the FCCI region where these transitions occurred with selected elements at low atomic fractions. A zoom-in view of this region is shown in Fig. 3b. The U profile indicated a higher concentration at the FCCI interface, followed by a sharp decline with only a small amount diffusing into the cladding. In contrast, the Zr profile showed minimal changes within the fuel at high atomic fractions. Other elements, such as Sm, Np, Pu, Si, and Am exhibited high concentrations in the fuel region near the FCCI interface and significant diffusion into the cladding at approximately 4 μm depth. Cladding elements such as Ni, Fe, and Cr, also clustered near the FCCI interface.

This detailed analysis provides insights into the diffusion patterns and interactions of various elements at the FCCI interface. The majority of the fuel side at the interface was Zr, instead of U. Additionally, consistent with the observations in Fig. 2, Am and Sm, each with an atomic fraction of <20 %, exhibited concentration profiles similar to Ni at the FCCI region. This suggests that Am and Sm may form compounds with Ni.

Meanwhile, Fe-rich agglomerates formed in the cladding near the FCCI interface. The segregation of Fe suggests a depletion of Fe in regions where Am, Sm, and Ni were concentrated, highlighting the complex chemical interactions occurring at the interface. Additionally, there was no significant diffusion of U and Pu into the cladding, indicating that these elements remained largely confined to the fuel region.

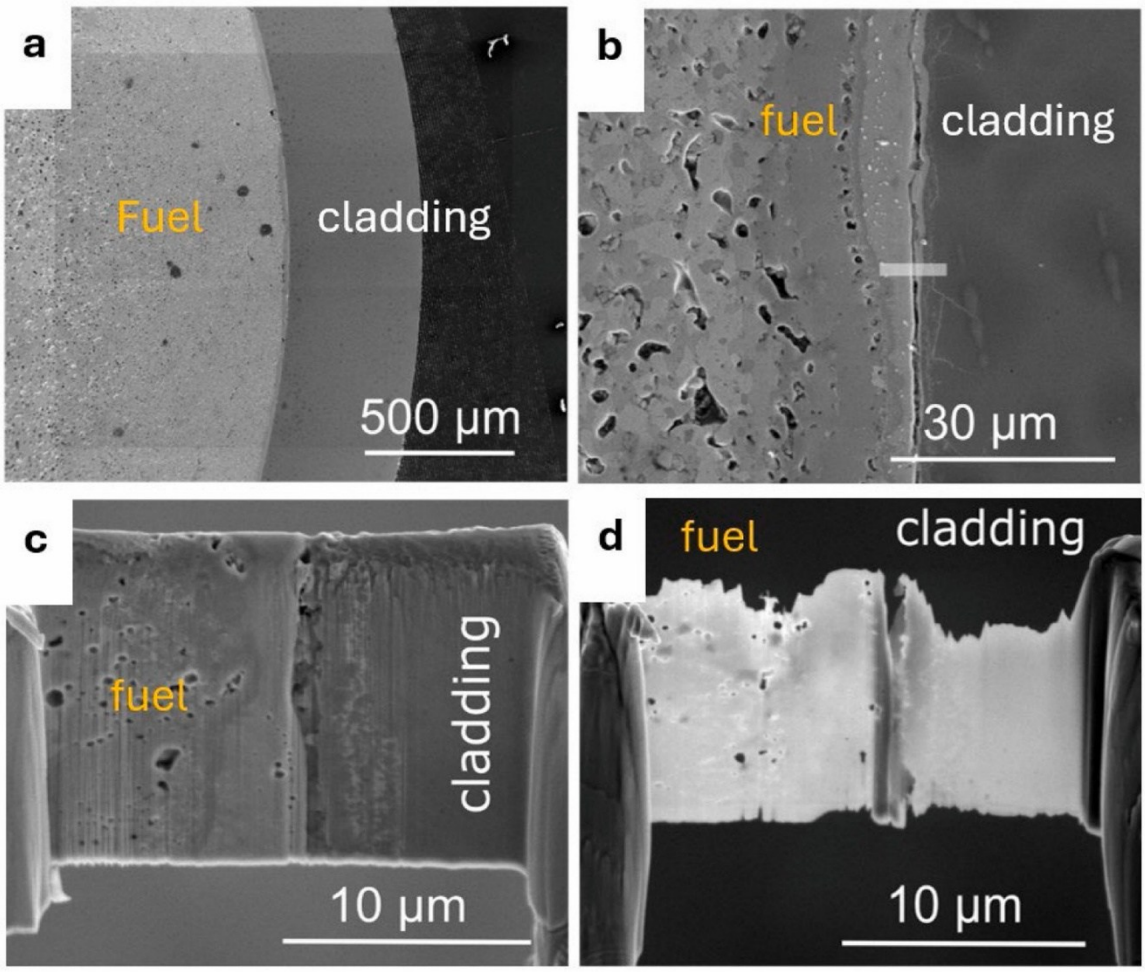

Figure 1. The SEM images of (a) the fuel AIM1 cladding, and the FCCI interface, (b) the location for first TEM lamella extraction, (c) The TEM lamella before thinning, and (d) the thinned lamella ready for TEM characterization

Fig. 3b provides a close-up view of the distribution of Am, Sm, U, Pu, and Np within the black box region. This detailed examination confirmed that these elements exhibited similar distribution patterns. The concentrations of Am and Sm were significantly higher than those of Np, U, and Pu inside cladding.

Fig. 4 presents a BF-TEM image along with the corresponding diffraction patterns from selected regions within the cladding, providing a detailed view of the microstructural and phase variations at different distances from the fuel-cladding interface.

Diffraction patterns obtained from the two regions, a and b, are displayed in Fig. 4. Corresponding to the BF-TEM image in Fig. 4, the region a was about 3–4 um away from the fuel-cladding interface while the region b was slightly less far.

Region 'a': Located farther from the interface, about 3–4 µm into cladding, region 'a' was devoid of Am and Sm. The diffraction pattern for this region reveals an FCC (face-centered cubic) structure viewed along the [110] direction, along with $M_{23}C_6$ carbides viewed along the [110] and [141] directions. Atomic fractions of Fe and Ni were approximately 65 % and 16 %,

respectively, as seen in Table 1, this region likely represented the Fe γ-phase matrix structure for stainless steel claddings [21].

Region 'b': Compared to region 'a', region 'b' was located closer to the interface where Am and Sm were concentrated. In this region, Am and Sm were 6 at% and 8 at%, respectively. The diffraction patterns from region 'b' were indexed as Hexagonal Closed Packed (HCP). The atomic fraction of Ni in this region was approximately 33 %, increased from 16 % in matrix region 'a'.

The BF-TEM image also showed various microstructural features, including white dots representing pores or voids, along with black stripes possibly for twinning in AIM1 cladding. Fig. 5 presents a detailed BF-TEM image of the fuel side, complemented by corresponding diffraction patterns from various regions.

Region 'c': Located furthest from the interface, region 'c' exhibited a diffraction pattern characteristic of the α-Zr phase, an HCP crystal structure. This phase was characterized by a high atomic fraction of Zr, approximately 92 at%, as detailed in Table 2. The diffraction patterns in the [− 15–43] and [01–14] directions further confirm the crystal structure.

Region 'd': Situated in the middle, region 'd' revealed diffraction patterns corresponding to the **δ-**UZr_2 phase, identified from [121] and [110] directions. The **δ-**UZr_2 phase adopted a hexagonal crystal structure with space group P6/mmm. This phase is typical for the UZr/Fe system and was characterized by a significant change in elemental composition compared to region 'c'. In Table 2, the atomic fraction of Zr decreased to 61 %, and the atomic fraction of U increased to 16 %. This differs from the stoichiometric **δ-**UZr_2 phase composition of 33 % U and 67 % Zr possibly due to the presence of other impurities.

Region 'e': The area closest to the interface, labeled as region 'e', presented challenges for analysis due to FIB damage as indicated by the amorphous halos.

Another TEM lamella was prepared, as described in Fig. 6. This lamella specifically focused on capturing the interactions and elemental distributions well inside the fuel side but near the fuel-cladding interface.

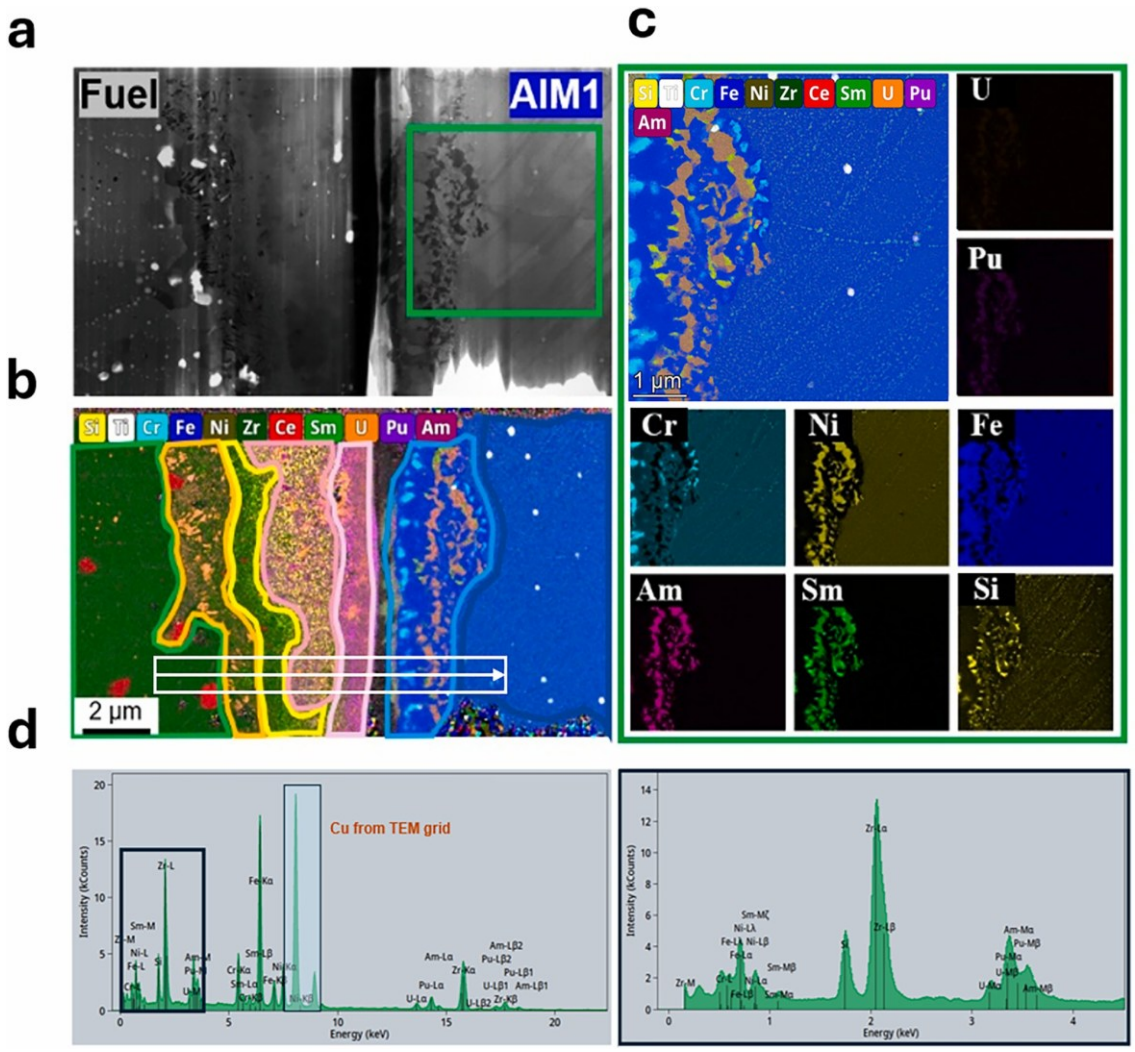

Figure 2. (a) An overview of the TEM bright field image of the FCCI region, (b) An overlayed STEM-EDS map shows the distribution of key elements, (c) The key elements overlayed and individually displayed from the cladding region indicated by the green box in (a), (d) Integrated spectrum of Am and Sm rich region in (c).

The STEM-EDS mapping was conducted on the second lamella, providing a comprehensive analysis of the elemental distributions. The elemental atomic percentages in Table 3 for region f were consistent with those in Table 2 for region e, confirming that both regions were within the same structural zone. The diffraction pattern, shown in Fig. 7, revealed that the phase in this region was a Zr(Si, U) fcc phase. This finding filled the gap from the previous lamella analysis, confirming the formation of a stable phase involving Zr, Si and U. The atomic fraction of Zr in this region was approximately 74 %. Lanthanide fission products are bonded with a Zr-rich compounds layer on the opposite side to the cladding.

4. Discussion

4.1.Phases identification

As the TEM results showed, many phases formed in the FCCI region due to the interdiffusion between the fuel and cladding. The complexity of these phases arose from the numerous elements present both in the fuel and AIM1 cladding.

4.1.1. Cladding microstructural analysis

Fe γ-phase with $M_{23}C_6$ Carbides: Located 3–4 μm from the interface in cladding, as seen in Fig. 4, this region displayed an FCC matrix structure with $M_{23}C_6$ carbides, typical of the Fe(Ni) γ-phase structure. The presence of $M_{23}C_6$ carbides, known for their high-temperature stability, suggests that the cladding maintained its integrity in these regions [22–24]. This region is free of Am and Sm.

Fe-Ni HCP Phase: Situated nearer to the interface, shown in Fig. 4, this region was rich in Am and Sm. The diffraction pattern for this area revealed an HCP structure, suggesting a notable transformation from the FCC matrix. This change correlates to the reduction of Fe and the presence of Am (7 at%) and Sm (5 at%) [25–27]. The formation of the Fe-Ni **HCP** phase could potentially affect the hardness, ductility, and resistance to corrosion of the AIM1 alloy.

4.1.2. Fuel microstructural analysis

Zr(Si, U) FCC Phase: The formation of the zirconium-rich FCC phase that contains Si and U near the FCCI interface can be related to the fabrication of the fuel slug during which Si was introduced as impurity from the casting quartz tube [16]. The FCC-Zr phase was studied before at the FCCI interface and referred to as "Zr rind" [28,29].

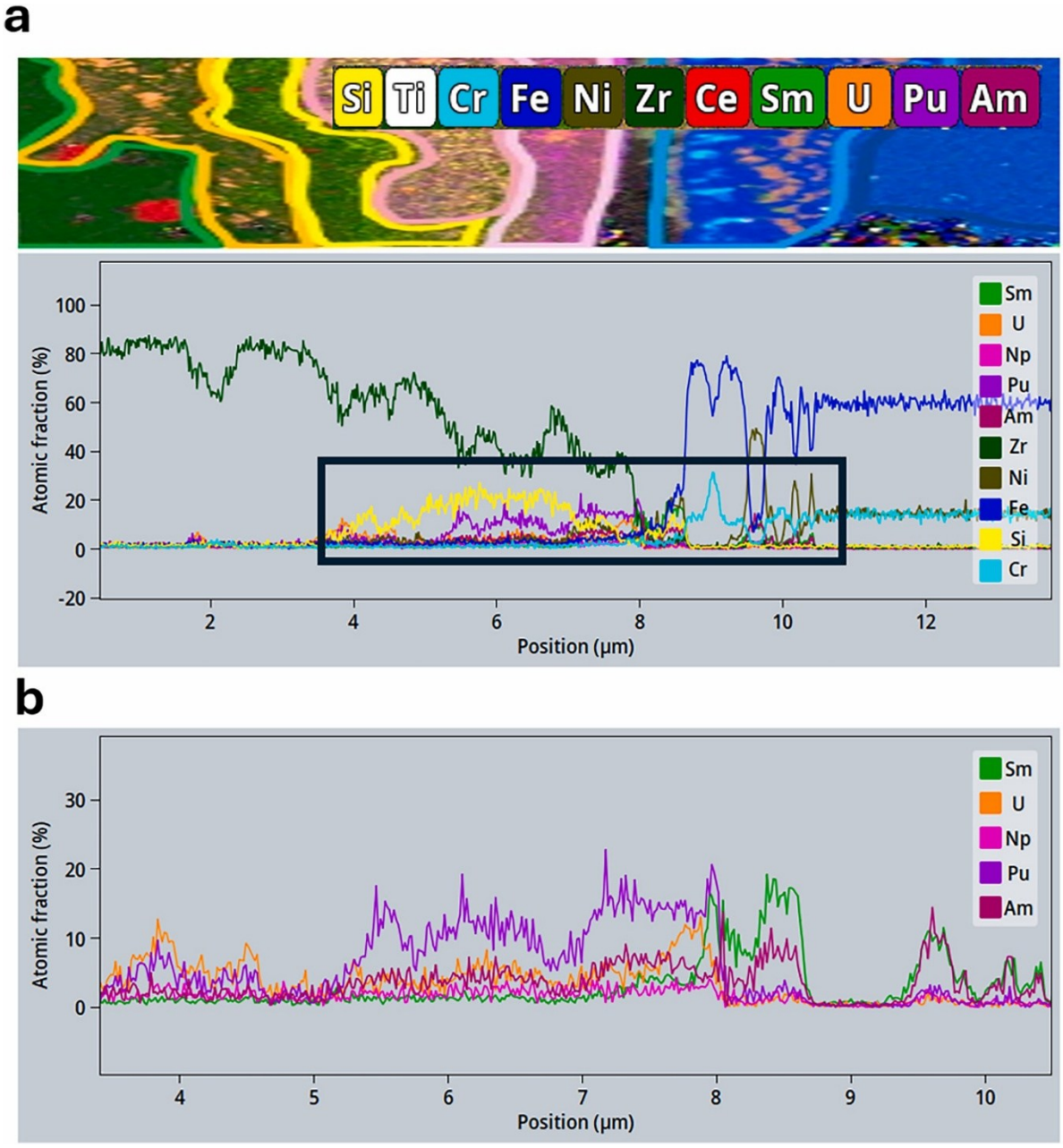

Figure 3. (a) STEM-EDS Line profile of elements from fuel to cladding, referring to the white arrow in Fig. 2c. (b) A close-up distribution profiles of the boxed region in (a) for Sm, U, Np, Pu, and Am at FCCI interface.

The formation of the FCC-Zr phase in this irradiated fuel sample could be related to irradiation effects [28] and/or mechanical constraints [30].

δ-UZr_2 Phase: Situated in the deeper region next to Zr(Si, U) FCC Phase, the diffraction pattern in Fig. 5 reveals a **δ-**UZr_2 phase. This phase is typical for the U-Zr system [31] and is characterized by a significant change in elemental composition compared to the regions farther

from the interface. The atomic fraction of Zr dropped to 61 %, while the atomic fraction of U increased to 16 %. The **δ-**UZr_2 phase is known to be the only intermetallic phase in the U–Zr system and many studies have investigated its formation mechanism and properties [32–35].

α-Zr **Phase**: Located furthest from the interface, this region shown in Fig. 5 exhibited a diffraction pattern indicative of the α-Zr phase. This phase was characterized by a high atomic fraction of Zr, approximately 92 %, as detailed in Table 2. Zr-rich layer at the interface were reported before to have a stable α-phase structure [36].

These observations provide a comprehensive understanding of the microstructural phase information at the FCCI region. The interplay of various elements and the resulting phase formation are critical for predicting the steady state fuel performance and hold values for advanced reactor designs with minor actinide transmutation [37].

4.2.Pu, Am, and Sm penetration into cladding

Pu, Am and Sm exhibit significant diffusion into the cladding due to irradiation-enhanced atomic mobility and their ability to form intermetallic phases with cladding constituents.

In contrast, Cr depletion in the cladding is likely driven by segregation effects and interactions with Am and Sm. This redistribution of Cr could weaken the cladding's structural integrity over time.

Fig. 8a shows that approximately 10–15 % of Am, in atomic percentage, was present at a depth of around 2 µm within the fuel side of FCCI region, creating a continuous distribution. On the cladding side,

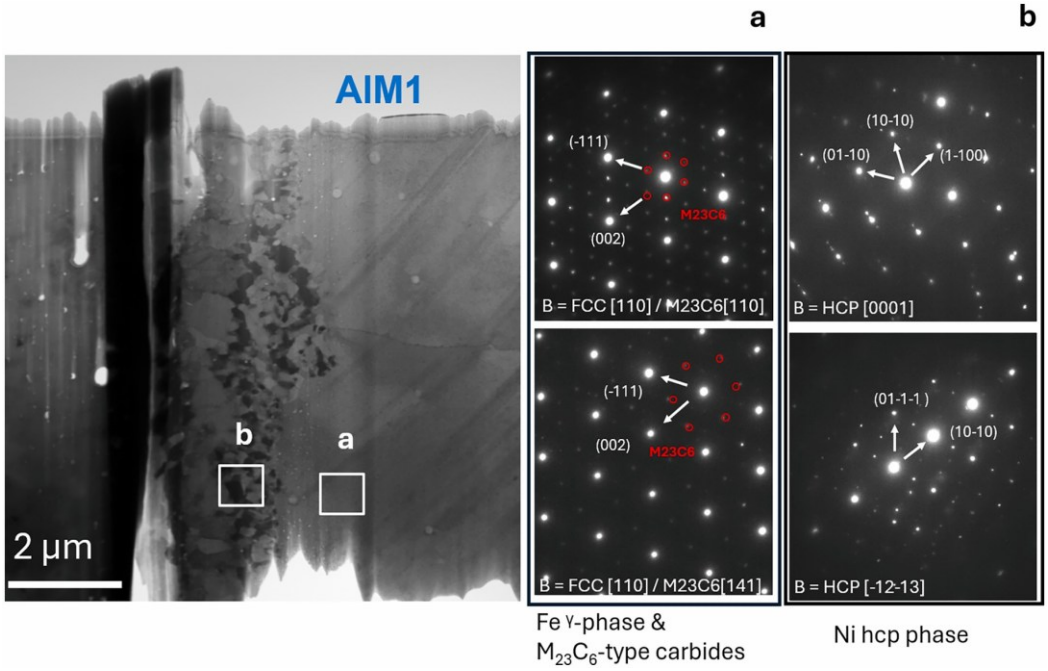

Figure 4. BF-TEM image of the AIM1 cladding, with selected regions 'a' and 'b' marked. Diffraction patterns of region 'a' indicate an FCC matrix structure and M23C6 carbide precipitates. Diffraction patterns of region 'b', closer to the interface and rich in Am and Sm, show a Hexagonal Close-Packed (HCP) crystal structure.

Table 1. Atomic fraction of the elements in region a and b.

	Si	Ti	Cr	Mn	Fe	Ni	Sm	U	Np	Pu	Am
Region a	0.76	0.14	15.00	3.11	65.09	15.77	0	0.03	0.03	0.03	0.04
Region b	2.11	0	6.32	1.87	41.72	32.9	8.29	0.13	0.23	0.77	5.66

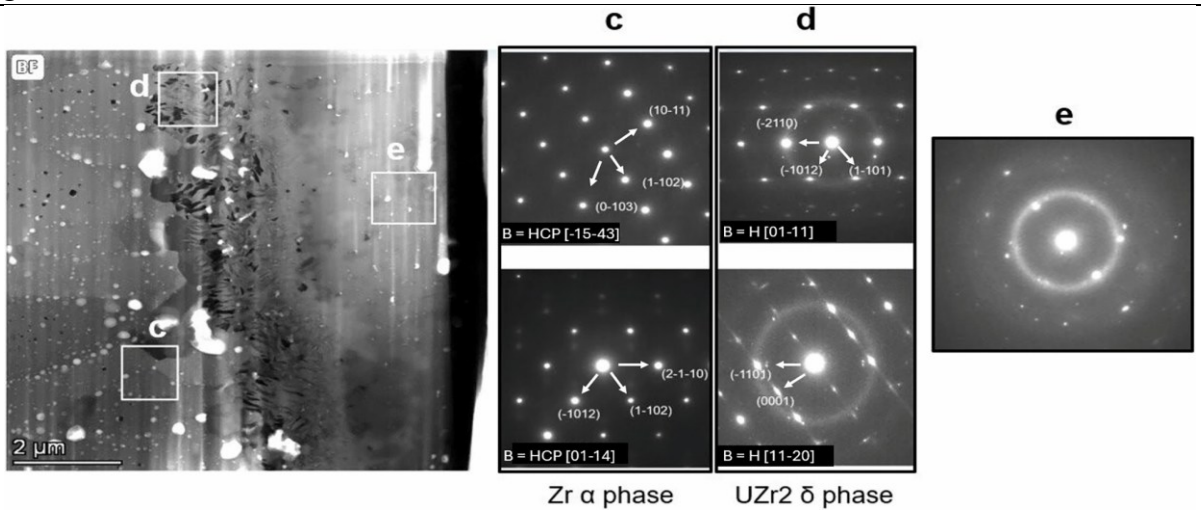

Figure 5. BF-TEM image of the fuel side with regions 'c', 'd', and 'e' marked. The diffraction pattern of region 'c' shows the α-Zr phase. The diffraction pattern of region 'd' indicates the δ-UZr2 phase. The diffraction pattern of region 'e' shows amorphization from FIB damage.

Table 2. Atomic fraction of the elements in regions c, d, and e.

	Si	Ti	Cr	Mn	Fe	Ni	Zr	Sm	U	Np	Pu	Am
Region c	0	0.15	0.03	0.02	0.56	0.58	97.64	0	0.12	0.19	0.37	0.34
Region d	6.87	0.07	0.31	0.25	2.61	2.43	60.54	0.17	16.00	1.48	8.39	0.88
Region e	6.78	0.07	0.31	0.25	2.65	2.47	60.52	0.17	16.09	1.41	8.43	0.86

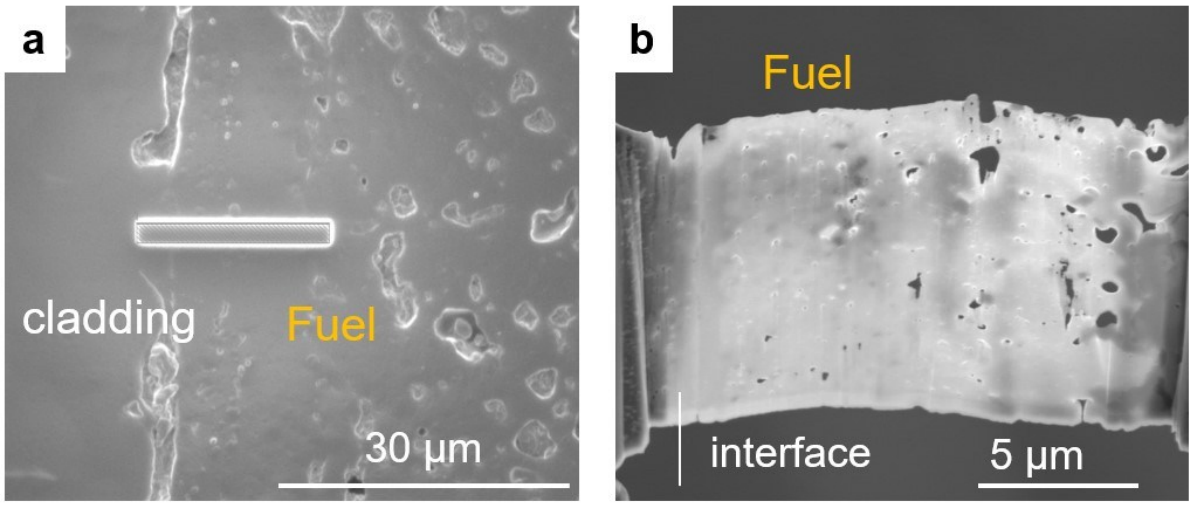

Figure 6. (a) SEM image of a marked location for the second lamella, (b) The second lamella after thinning.

Table 3. the elemental atomic fraction in region f

	Si	Ti	Cr	Mn	Fe	Ni	Zr	Sm	U	Np	Pu	Am
Region f	13.55	0.25	0.07	0.04	1.15	1.03	73.97	0.20	2.47	0.36	5.08	1.83

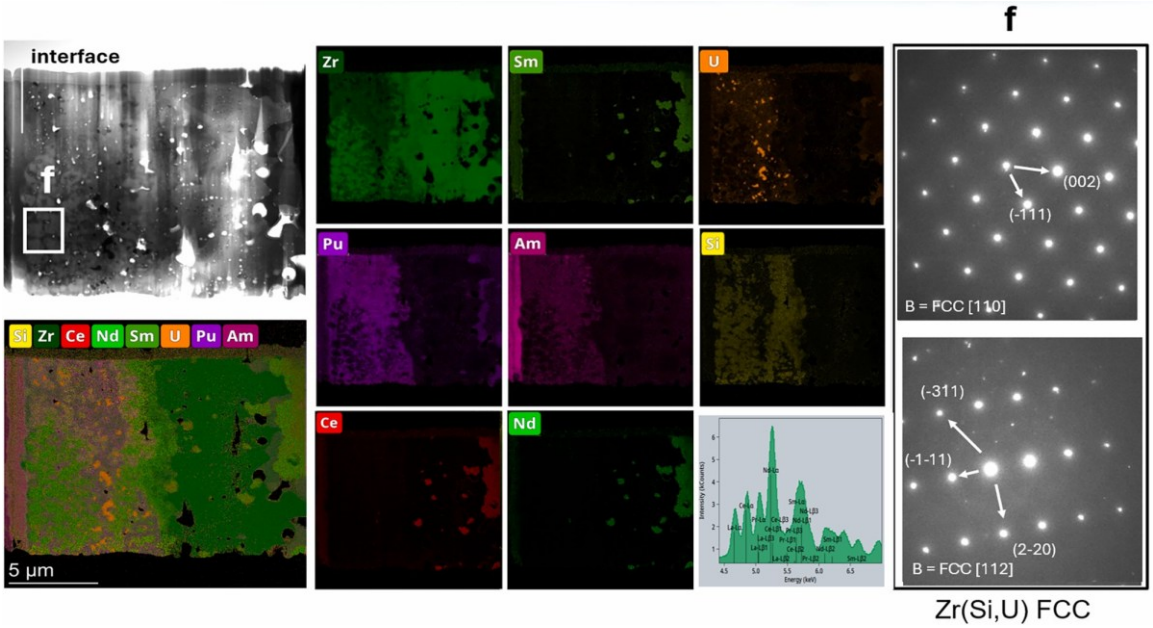

Figure 7. BF-TEM image of the second lamella with corresponding STEM-EDS mapping of key elements, spectrum for lanthanide fission products, and indexed diffraction patterns collected from region f in BF-TEM image

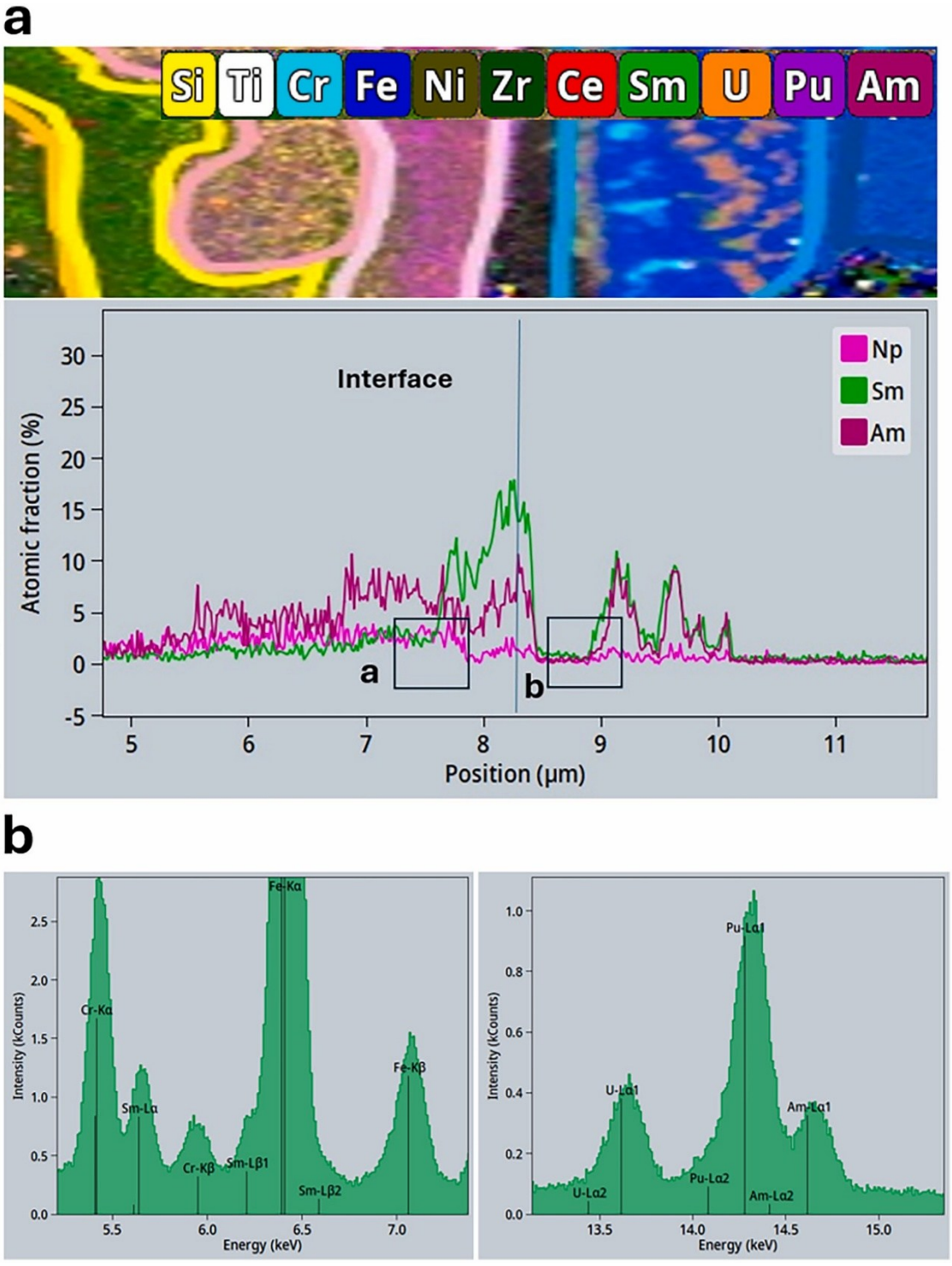

Figure 8. (a) One-dimensional integrated Sm, Am and Np distribution throughout the region from fuel to cladding. (b) Integrated spectrum of U, Pu, Am, Sm, Fe and Cr within the same region.

the penetration depth of Am was about 4 μm, where it formed a new compound with Sm, Ni, and Si, reaching a maximum concentration of about 10 % in atomic percentage. By integrating

the peak areas on STEM EDS spectrum from a single dataset, it was determined that the ratio of Am diffused into the cladding to the amount present in the fuel was approximately 1:5. This indicates that a significant portion of Am remained within the fuel, with only a smaller fraction penetrating the cladding material. This diffusion behavior suggests that Am had relatively moderate mobility within the fuel-cladding interface, possibly influenced by the presence of Zr compounds. The retention within the fuel matrix is likely due to strong chemical bonding with other alloying elements, such as U and Pu, which restrict mobility compared to the diffusion of Sm.

As seen in Fig. 2 STEM EDS maps, Am and Sm from the fuel were two elements that noticeably penetrated into the cladding. The distribution patterns of Am, Pu in the fuel were similar, suggesting strong bonding between these two elements [38]. Sm, a solid fission products, exhibited a different diffusion mechanism. As shown in Fig. 8a, it was concentrated more than Am at the interface within the fuel, indicating that Sm diffused faster than Am. Additionally, the fact that Sm did not form compounds with Pu may further enhance its diffusion.

When Am and Sm diffused into the cladding to a depth of 2–3 μm, they formed Am and Sm rich precipitates. The distribution patterns of Am and Sm closely resembled those of Ni and Si as seen in Figs. 2 and 3, suggesting the formation of compounds involving these elements. Studies have shown that silicon-nickel intermetallic compounds can form under similar conditions [39], supporting the likelihood of such compound formations involving Am and Sm. Our findings not only align with previous study [16] but also provides further insights into the specific diffusion behaviors and compound formation involving Sm and Am. We observed Sm and Am forming clusters with Ni and Si near the interface, with penetration depths limited to 2–3 μm, differing from previous study [16]. These differences may be attributed to local variations in thermo-irradiation conditions and fuel composition even on the same fuel cross section sample. Moreover, ref. [16] emphasized the dissolution of Am into major fuel phases and its role in forming complex compounds at the fuel periphery. Our results complement these findings by identifying additional interactions between Am, Sm, Ni, and Si, forming intermetallic compounds. These findings provide a more detailed understanding of how MA influences FCCI.

The depletion of Cr and Fe observed in the EDS maps in Fig. 2 corresponds to regions where Am and Sm are concentrated in the cladding. This suggests that local Fe segregation may be influenced by the presence of MA, possibly leading to the formation of distinct phases involving Ni, Fe, Si, Am, and Sm. The work by McDeavitt also indicated that Fe can form intermetallic phases with various fission products and MA [40].

In contrast, Np showed a very small presence on both sides of the fuel and cladding, as illustrated in Fig. 8a and b. This limited diffusion of Np was advantageous, as it reduced the likelihood of Np-induced degradation in the cladding material.

Additionally, the Np concentration was only high in the U-rich phase, resulting in a low Np concentration in the Zr-rich phase, while Am exhibited the opposite behavior [19]. These factors together explain why very little Np was observed in the FCCI region.

Furthermore, the differences in diffusion behaviors between Am and Np emphasize the need for tailored strategies to manage each element within the nuclear fuel cycle. For instance, while

Am requires considerations for its moderate mobility and potential for compound formation at FCCI regions, Np does not have negative impacts on FCCI between U- Pu-Zr fuel and AIM1 cladding.

The formation of Am-Sm-Ni-Si compounds could cause embrittlement at the affected region and lead to cladding wastage that affects the mechanical robustness of cladding.

4.3.Zr-rich compounds layer

The Zr compound layer could be an artifact of the fabrication process, where Zr from the charge as partially stabilized by oxygen, leading to the formation of a Zr-rich layer [7]. Huang, K. et al. discussed the role of Zr-rich compounds layer as a possible diffusion barrier for FCCI in U-Mo nuclear fuels[18]. Several detailed examinations of fuel-cladding interaction layers in irradiated U-Zr and U-Pu-Zr fuel elements also underscore the role of Zr compound layer in stabilizing these interfaces and preventing the migration of lanthanide fission products [28–29, 41–44].

Our previous EPMA study revealed a Zr layer, around 20 μm thick, at the FCCI interface [16]. Fig. 5 and Table 2 reveal an over 90 % atomic concentration of Zr far away from the FCCI interface. Closer to the interface, Zr atomic concentration dropped to 70 % and 50 %, as depicted in Figs. 5 and 6 and Tables 2 and 3.Lanthanide fission product other than Sm, as represented by Ce mapping in Fig. 2, are well stopped or confined in the Zr rich layer. However, no Zr diffused into the cladding, despite the high concentration at the interface.

4.4.Comparison with un-doped U-Pu-Zr fuels

The inclusion of MA such as Am and Np introduces significant differences in FCCI compared to un-doped U-Pu-Zr fuels. MA form unique phases such as Am-Ni-Si-Sm-rich compounds that were not observed in un-doped fuels. Am and Sm penetrated much deeper into the cladding than U and Pu.

Compared to literature data on un-doped U-Pu-Zr fuels, the diffusion profiles observed in this study reveal a greater penetration depth for MA such as Am into the cladding, in conjuction with Sm, a lanthanide fission product, and along with the formation of distinct intermetallic compounds. Since Sm is a fission product and Am is intentionally added into the U-Pu-Zr fuel for actinide transmutation, the similar diffusion behavior and phase formation between these two elements requires further investigation.

4.5.Overview of FCCI mechanism

Fig. 9 provides a diagram representing the FCCI and phase formation in the MA-bearing U-Pu-Zr fuel and AIM1 cladding. The diagram includes chemical interaction free zone of both fuel and cladding, the fuel- cladding interface, and the phases formation across the fuel-cladding interface:

- **Cladding in the FCCI region**: The cladding in the FCCI region exhibits the segregation of elements such as Ni, Am, Sm, and Fe. According to the diagram in Figs. 2 and 8, Ni-Am-

Sm clusters were formed, with Si and Fe possibly playing roles as well. Meanwhile, Cr segregation led to the formation of Cr clusters near the interface.

- **Fuel in the FCCI region**: The fuel in the FCCI region dissociated into Am, Zr, Zr-Si-Pu-U, and U-Pu phases. The formation of these phases indicates complex chemical interactions and phase transformations during reactor operation.

The schematic (Fig. 9) helps visualize the chemical interactions and elemental redistributions occurring at the FCCI interface.

5. Conclusion

This study conducted an in-depth analysis of the FCCI between a MA- bearing U-Pu-Zr metallic fuel and AIM1 cladding irradiated in Phenix fast reactor to 9.5 % Chemical Interaction FIMA burnup at approximately 550 ˚C cladding temperature. The objective was to understand the microstructural and elemental interactions at the FCCI interface on a smaller length scale to increase confidence in fuel performance modeling and guide the design of future MA-bearing fuels. Our findings are summarized as following:

1. **Zr-rich compounds Layer**: The formation of a Zr-rich compounds layer at the fuel-cladding interface, likely originating from the fuel fabrication process, played a modest role in metigating FCCI. This layer can efficiently prevent most lanthanide fission products from reaching the FCCI interface and reacting with cladding consitituents. However, it cannot stop Am and Sm in a similar manner. Additionally, maintaining the integrity of the Zr compounds layer during reactor irradiation can be challenging.
2. **Diffusion of Minor Actinides**: Am and Sm diffuse into the cladding, forming new phases with Ni and Si, while Np remaines mostly in the fuel with minimal presence in FCCI region.
3. **Phase Transformations**: The formation of Zr(Si, U) FCC and the **δ-**UZr_2 phase at the FCCI interface reduces lanthanide accumulation on the AIM1 cladding inner surface.
4. **Implications for Fuel Performance**: Limited cladding wastage (everal μm) suggests benign FCCI behavior for the investigated MA- bearing U-Pu-Zr fuel with AIM1 cladding.

Fig. 9.

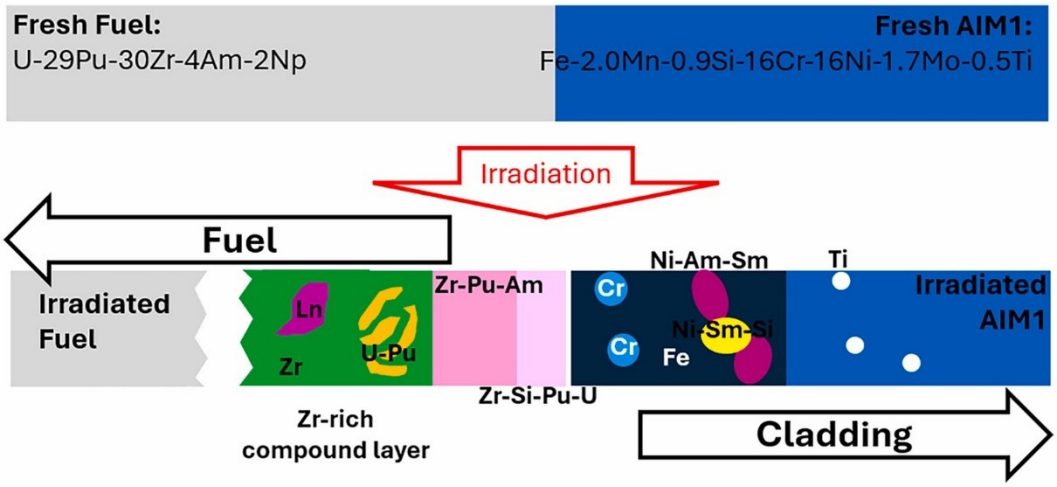

Figure 9. Schematic diagram of FCCI interface region between MA-bearing U-Pu-Zr fuel and AIM1 cladding, showing the formation of multiple phases after reactor irradiation.

CRediT authorship contribution statement

Di Chen: Writing – review & editing, Writing – original draft, Methodology, Formal analysis, Data curation. **Jatuporn Burns:** Writing – review & editing, Data curation. **Karen E. Wright:** Methodology, Data curation. **Daniele Salvato:** Formal analysis, Data curation. **Tiankai Yao:** Writing – review & editing, Supervision, Resources, Methodology, Funding acquisition, Data curation, Conceptualization. **Luca Capriotti:** Writing – review & editing, Validation, Supervision, Resources, Methodology, Funding acquisition, Conceptualization.

Declaration of Competing Interest

The authors declare that there are no known conflicts of interest associated with this publication.

All co-authors have approved the manuscript, and the study was conducted without any commercial or financial relationships that could be construed as potential conflicts of interest.

We confirm that the manuscript has not been published elsewhere and is not under consideration for publication in any other journal.

Acknowledgement

Authors acknowledge U.S. Department of Energy, Office of Nuclear Energy, Advanced Fuels Campaign for fuel sample preparation and irradiation. The post irradiation examination is supported by the U.S. Department of Energy, Office of Nuclear Energy under DOE Idaho Operations Office Contract DE-AC07- 051D14517 as part of the Nuclear Science User Facilities. Tiankai Yao and Di Chen acknowledge the financial support of Laboratory Directed Research and Development project (22A1059-094FP) for data analysis and manuscript preparation.

Data availability

Data will be made available on request.

References

[1] S.L. Hayes, B.A. Hilton, M.K. Meyer, G.S. Chang, F.W. Ingram, S. Pillon, N. Schmidt, L. Leconte, D. Hass, U.S. plans for actinide transmutation fuel development, Trans. Am. Nucl. Soc. 87 (2002) 353.

[2] Report to Congress on the Advanced Fuel Cycle Initiative: The Future Path for Advanced Spent Fuel Treatment and Transmutation Research, U.S. Department of Energy Office of Nuclear Science and Technology, Jan. 2003.

[3] M. Salvatores, Nuclear fuel cycle strategies including partitioning and transmutation, Nucl. Eng. Des. 235 (2005) 805–816.

[4] H.E. Garcia, M.J. Lineberry, S.E. Aumeier, H.F. McFarlane, Proliferation resistance of advanced sustainable nuclear fuel cycles, in: Global 2001 International Conference on: "Back-end of the Fuel Cycle: from Research to Solutions, Paris, 2001, 9-13 Sep. 2001.

[5] H.M. Chichester, S.L. Hayes, K.J. McClellan, J. Paul, M. Masson, S.L. Voit, F. Delage, Overview of the FUTURIX-FTA irradiation experiment in the Ph_enix reactor, in: GLOBAL 2015 Conference, Paris, 2015, pp. 20–24. Sepp2015.

[6] J.M. Harp, H.J.M. Chichester, L. Capriotti, Baseline Postirradiation Examination of the FUTURIX FTA Experiment, Idaho National Laboratory, 2016. ReportINL/LTD- 16-40088.

[7] J.M. Harp, L. Capriotti, H.J.M. Chichester, Postirradiation examination of FUTURIX-FTA metallic alloy experiments, J. Nucl. Mater. 515 (2019) 420–433.

[8] D.D. Keiser, Fuel cladding chemical interaction in metallic sodium fast reactor fuels: a historical perspective, J. Nucl. Mater. 514 (2019) 393–398.

[9] D.L. Porter, G.L. Hofman, B.R. Seidel, L.C. Walters, Factors controlling metal fuel lifetime, Int. Conf. Reliab. Fuels Liq. Met. Factors, Tuscon, AZ (1986).

[10] Y.H. Sohn, M.A. Dayananda, G.L. Hofman, R.V. Strain, S.L. Hayes, Analysis of constituent redistribution in the g (bcc) U-Pu-Zr alloys under gradients of temperature and concentrations, J. Nucl. Mater. 279 (2000) 317–329.

[11] Y.S. Kim, G.L. Hofman, S.L. Hayes, Y.H. Sohn, Constituent redistribution in U-Pu-Zr fuel during irradiation, J. Nucl. Mater. 327 (2004) 27–36.

[12] Y.S. Kim, S.L. Hayes, G.L. Hofman, A.M. Yacout, Modeling of constituent redistribution in U-Pu-Zr metallic fuel, J. Nucl. Mater. (2006) 17–28.

[13] J. Galloway, C. Unal, N. Carlson, D. Porter, S. Hayes, Modeling constituent redistribution in U-Pu-Zr metallic fuel using the advanced fuel performance code BISON, Nucl. Eng. Des. 286 (2015) 1–17.

[14] S. Br_emier, P. P€oml, L. Capriotti, J. Himbert, V.V. Rondinella, H. Ohta, T. Ogata, Electron microprobe examination of irradiated metallic fuel containing rare earth and minor actinide elements, proc, Am. Nucl. Soc 117 (2017) 590–593.

[15] K.E. Wright, D.D. Keiser, J.R. Kennedy, R.G. Pahl, L.C. Walters, Fuel-cladding chemical interactions in U-Pu-Zr metallic fuels, J. Nucl. Mater. 393 (2019) 110–118.

[16] K.E. Wright, J.M. Harp, L. Capriotti, Electron probe microanalysis of irradiated FUTURIX-FTA U-Pu-Zr alloy with added minor actinides, Journal of Nuclear Materials (2019) 526.
[17] J.R. Kennedy, FUTURIX-FTA Metal Alloy Fuel Fabrication and Characterization Report, INL/EXT-07-12234, Idaho National Laboratory, 2007.
[18] A. Courcelle, C. Bisor, E. Piozin, M. Kountchou, Evolution under irradiation of optimized austenitic steel for Gen-IV reactors. Impact on fuel cladding properties and performances, Eur. Phys. J. Conf. 115 (2016) 04003.
[19] E. Curtet, P. Olier, E. Curtet, S. Urvoy, M. Bono, et al., in: Fabrication and characterization of 15Cr-15Ni austenitic steel cladding tubes for sodium fast reactors. *ICAPP'2019 - The International Congress on Advances in Nuclear Power Plants, May*, Juan-Les-Pins, France, 2019.
[20] T. Yao, X. Liu, Y. Wang, F. Teng, D.J. Murray, M. Meyer, M.T. Benson, L. Capriotti, Transmission electron microscopy based characterization of a U-20Pu-10Zr fuel irradiated in experimental breeder Reactor-II, J. Nucl. Mater. 568 (2022) 153846 chrome-extension://efaidnbmnnnibpcajpcglclefindmkaj/, https://www.osti.gov/servlets/purl/1923683.
[21] P. Zhang, H. Jian, L. Yin, J. Liu, Z. Cai, Y. Tong, Corrosion resistance and mechanical properties of Cr-rich 316 stainless steel coatings fabricated by the TIG process using flux-cored wires, J. Nucl. Mater. 29 (8) (2024).
[22] Y. Zhao, W. Liu, T. Zhang, Z. Sun, Y. Wang, Y. Fan, B. Dong, Assessment of the correlation between M23C6 precipitates and pitting corrosion resistance of 0Cr13 martensitic stainless steel, Corros. Sci. 189 (2021) 109580.
[23] J.H. Baek, C.H. Han, W.G. Kim, T.K. Kim, J.H. Kim, S.H. Kim, C.B Lee, Effects of boron addition on creep and microstructure in 9Cr-0.5Mo-2W-V-Nb-B steels for a SFR fuel cladding, Korea, Republic of: N. (2009).
[24] T.H. Lee, H.Y. Suh, J.H. Lee, Precipitation behavior of $M_{23}C_6$ carbides and its effect on mechanical properties of Ni-based Alloy 690, J. Nucl. Sci. Technol. 58 (1) (2020) 45–50.
[25] L. Dubrovinsky, N. Dubrovinskaia, W. Crichton, Pressure-induced fcc to hcp phase transition in Ni-based high entropy solid solution alloys, Phys. Rev. Lett. (2007) 98.
[26] F.X. Zhang, S. Zhao, K. Jin, H. Bei, D. Popov, C. Park, J.C. Neuefeind, W.J. Weber, Y. Zhang, Pressure-induced fcc to hcp phase transition in Ni-based high entropy solid solution alloys, Phys. Rev. Lett. 110 (2017) 011902.
[27] Y. Wang, C. Wu, Y. Liu, M. Tian, X. Lu, X. Su, Insight into the FCC→HCP transformation in Co-rich Co-Cr-Fe-Mn-Ni high-entropy alloys, Metal. (Basel) 13 (2023) 504.
[28] M.T. Benson, T. Yao, J.N. Zelina, F. Teng, D. Murray, F.D. Lemma, W.J. Williams, J. Zhang, W. Zhuo, The formation mechanism of the Zr rind in U-Zr fuels, J. Nucl. Mater. 572 (2022) 154057.
[29] T. Yao, L. Capriotti, J.M. Harp, X. Liu, Y. Wang, F. Teng, D.J. Murray, A.J. Winston, J. Gan, M.T. Benson, Lingfeng He, α-U and ω-UZr2 in neutron irradiated U-10Zr annular metallic fuel, J. Nucl. Mater. 542 (2020) 152536.

[30] Q. Jiang, Y. Chen, Q. Shuai, F. Liu, L. Li, C. He, H. Zhang, C. Wang, Y. Liu, Q. Wang, Fatigue-induced HCP-to-FCC phase transformation resulting in two FCC-Zr variants in pure zirconium, Mater. (Basel) 16 (18) (2023) 6215.
[31] B. Beeler, K. Mahbuba, Y. Wang, Magnetism and finite-temperature effects in UZr2: a density functional theory analysis, Front. Mater. 8 (2021).
[32] S. Irukuvarghula, S. Ahn, S.M. McDeavitt, Decomposition of the γ phase in as-cast and quenched U–Zr alloys, J. Nucl. Mater. 473 (2016) 35–44.
[33] C. Bhanu Basak, N. Prabhu, M. Krishnan, On the formation mechanism of UZr2 phase, Intermetallics 18 (9) (2010) 1707–1712.
[34] C.B. Basak, A.K. Poswal, Structure and stability of δ-UZr_2 phase in U-50wt% Zr alloy, Philosoph. Magaz. 102 (9) (2021) 787–802.
[35] A. Sen, M. Bachhav, X. Pu, F. Teng, T. Yao, J.P. Wharry, Irradiation effects on stability of δ-UZr2 phase in U-50 wt% Zr alloy, J. Nucl. Mater. (2020).
[36] S. Kaity, Investigation of Physico-Chemical Properties of Fast Reactor Metallic Fuels, PhD Thesis, Homi Bhabha National Institute, Mumbai, March 2021.
[37] Y. Xie, J. Zhang, X. Li, Lanthanide migration and immobilization in metallic fuels, Progr. Nucl. Energy 109 (2018) 266–278.
[38] H. Okamoto, Am-Pu (Americium-Plutonium), J. Phase Equilib. Diffus. 32 (2011) 575.
[39] B. Bokhonov, M. Korchagin, In-situ investigation of the formation of nickel silicides during interaction of single-crystalline and amorphous silicon with nickel, J. Alloy. Compd. 319 (1–2) (2001) 187–195.
[40] S.M. McDeavitt, Alloy waste forms for Metal Fission Products and Actinides Isolated by Spent Nuclear Fuel Treatment, Minerals, Metals and Materials Society, 1996.
[41] I. Colliard, et al., Metal-oxide cages open up strategy for processing nuclear waste, Nat. Chem. 14 (2022) 1357–1366.
[42] D.D. Keister, Fuel-cladding interaction layers in irradiated U-ZR and U-PU-ZR fuel elements, Argonne National Laboratory, January 23, 2006. Report No. ANL-NT- 240.
[43] D.D. Keiser Jr., E. Perez, T. Wiencek, Microstructural characterization of a thin film ZrN diffusion barrier in an As-fabricated U–7Mo/Al matrix dispersion fuel plate, J. Nucl. Mater. 465 (2015) 36–47.
[44] W.J. Williams, T. Yao, X. Pu, L. Capriotti, Characterization of micro-burnup treat irradiated U-22.5 at.% Zr and U-52.8 at.% Zr foils by transmission electron microscopy and X-ray diffraction, J. Nucl. Mater. 585 (2023) 154644